Materials Advances

ROYAL SOCIETY OF CHEMISTRY

PAPER

View Article Online
View Journal | View Issue

Cite this: *Mater. Adv.*, 2021, 2, 6641

Organic double D–π–A sensitizers based on 2,2′-(2,2 diphenylethene-1,1-diyl)dithiophene: π-conjugation fragment effect on the photovoltaic properties†

Pengjuan Zhou,[a] Bobing Lin,[a] Ran Chen,[a] Jianying Liang,[a] Zhongwei An,*[ab] Qiang Weng,*[a] Xinbing Chen [a] and Pei Chen[a]

Received 16th August 2021,
Accepted 30th August 2021

DOI: 10.1039/d1ma00728a

rsc.li/materials-advances

The development of new dye sensitizers to further reveal the influence of changes in structural components on the photovoltaic performance is of great significance to dye-sensitized solar cells (DSSCs). The propeller-shaped 2,2′-(2,2-diphenylethene-1,1-diyl)dithiophene (**DPDT**) unit was introduced to construct sensitizers for the first time. Three **DPDT**-bridged double D–π–A organic sensitizers (**A6**, **A8**, **A9**) were prepared by altering the π-conjugation fragment. The photophysical, electrochemical and photovoltaic properties of the sensitizers were systematically investigated to assess the role of the terminal fragment of dyes in DSSCs. The results show that, compared to the mono-anchoring congener **AZ6**, the di-anchoring sensitizer **A6** displayed a comparable power conversion efficiency (PCE = 8.21%) and a higher short-circuit current density (J_{SC}). Replacement of the terminal thiophene with a phenyl ring (**A9**) can effectively increase the photovoltage by 70 mV with an efficiency of 8.14%, which is 1.5 times higher than that of **A8** (5.36%) with 2-cyanoacrylic acid at the *meta*-position of the phenyl ring. These results indicate that the terminal fragments of sensitizers have a significant effect on the photovoltaic performance.

Introduction

The field of dye-sensitized solar cells (DSSCs) has grown at an alarming speed and significant achievements have been made in metal complex-sensitized[1,2] and pure organic dye-sensitized solar cells in the last three decades.[3–5] As a crucial assembly unit, sensitizers fundamentally affect the performance of DSSCs and have grown rapidly in recent decades.[6–8] Numerous ruthenium complex dyes and zinc porphyrin sensitizers with high efficiency such as CYC-B11[9] (11.5%), SM315[10] (13.0%), XW51[11] (11.1%), and so on have been reported. Among various dyes,[12,13] metal-free photosensitizers have also aroused great research interest due to the flexible molecular design, high molar extinction coefficients, and cost-effectiveness. In addition to the donor–π–acceptor (D–π–A) featured sensitizers,[14] new types of dyes have been developed to seek ideal sensitizers with the characteristics of being aggregation-resistant and having strong absorption. Recently, some studies have found that di-anchoring dyes[15,16] have a stronger affinity to photoanodes, are more stable than the corresponding mono-anchored dyes, and can provide more electron injection pathways.

However, compared with mono-anchoring dyes, di-anchoring dyes[17–19] usually suffer a decreased open-circuit voltage (V_{OC}) due to the change of the conduction band edge (E_{CB}) of TiO_2 and dark current. Therefore, more new fragment compositions were introduced into the di-anchoring dyes to overcome this shortcoming.[20–22] Recently, the light-emitting molecule tetraarylethylene[23] has attracted our interest, which can effectively promote the orderly aggregation of dyes without introducing aggregation-induced emission (AIE) characteristics. Since the Su group[24] first introduced the tetraphenylethylene (TPE) core into X-shaped dyes, more dyes have been introduced into this fragment at different sites. For example, the Lin group[25] synthesized a series of di-anchoring TPE-tethered YL dyes, providing a stronger ability to suppress charge recombination compared to the congener dyes. Recently, Zheng and co-workers found that different triarylethylene (TAE)[26] units, when used as a π-spacer fragment of dyes, have an impact on photovoltaic properties. The DPTP unit has similar AIE properties, which may be more beneficial to the

[a] *Key Laboratory of Applied Surface and Colloid Chemistry (MOE), Shaanxi Key Laboratory for Advanced Energy Devices, Shaanxi Engineering Lab for Advanced Energy Technology, School of Materials Science and Engineering, Shaanxi Normal University, Xi'an 710062, P. R. China. E-mail: gmecazw@163.com*
[b] *Xi'an Modern Chemistry Research Institute, Xi'an, 710065, China*

† Electronic supplementary information (ESI) available. See DOI: 10.1039/d1ma00728a

light absorption of dyes due to the electron-rich characteristics of thiophene. Therefore, it is still potentially valuable to introduce the DPTP unit into dye molecules.

Up to now, di-anchoring dyes[27–30] have not been extensively studied due to the difficulties in the design and synthesis of di-anchoring dyes. It is easy to find that little attention was paid to the modulation of the π-spacer fragment, which dramatically affected the optical properties and the interfacial charge recombination. Thiophene and phenyl rings are the most commonly used π-spacer components. Dyes containing thiophene as a π-spacer component always display a higher J_{SC} value but a lower open-circuit voltage,[31,32] while dyes with phenyl as a π-spacer component usually exhibit opposite results.[33–35] By inserting an additional terminal phenyl ring, the reported dyes **GY50**[36] and **2**[37] can greatly suppress the charge recombination and significantly improve the V_{OC} and J_{SC}. Simultaneously, the position of the acceptor in sensitizers has an influence on the binding mode and photovoltaic properties.[38] For instance, Galoppini *et al.*[39] reported that the anchor group of sensitizers in the meta position (**m-ZnTCPP**) favored a planar binding mode to the metal oxide surfaces. D'Souza and Gao[40,41] revealed that dyes with a *para-* or *meta*-position acceptor showed better DSSC performance than dyes with an *ortho*-position acceptor. However, related investigations are still scant, especially in metal-free di-anchoring dyes.

Based on the above background, we introduced the propeller-shaped DPDT unit into double D–π–A sensitizers (**A6**, **A8**, **A9**) for the first time and connected it with different terminal fragments of dyes (Fig. 1). The cyclic thiourea functionalized triphenylamine was selected as the donor unit due to its excellent optical characteristics and the ability to inhibit charge recombination.[42] Bithiophene or 2-phenylthiophene was selected as the π-spacer with cyanoacrylic acid as the acceptor at the *meta-* or *para*-position of the phenyl ring. The dyes are applied in DSSCs to understand which is the dominant factor affecting the V_{OC} of double D–π–A sensitizers: the conduction band edge (E_{CB}) of TiO_2 or the ability to suppress the dark current? In addition, it is important to clarify that the different geometric configurations caused by the positions of the *para-* or *meta*-anchoring group of benzene may affect the loading mode of dyes on TiO_2 film. The reported D–π–A sensitizer **AZ6** was synthesized as a reference. The photophysical, electrochemical and photovoltaic properties of the dyes were studied systematically. In particular, the synthetic method provides more space and feasibility for further modulation of the tetraarylethylene fragment.

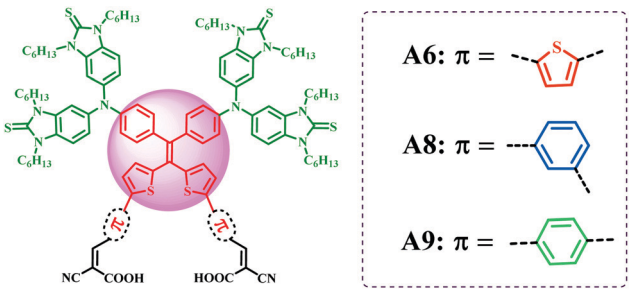

Fig. 1 Chemical structures of sensitizers **A6**, **A8**, and **A9**.

Results and discussion

Material synthesis and characterization

The synthetic routes of **A6**, **A8**, and **A9** are shown in Scheme 1. The raw material $C_6S_2TPAB(OH)_2$ was synthesized according to our previously reported method.[42] Intermediates **3a–3c** and **4a–4c** were synthesized *via* Suzuki coupling. The target dye molecules **A6**, **A8**, and **A9** were obtained from **4a–4c** *via* the Knoevenagel condensation reaction. All of the new compounds were characterized by ^{1}H NMR, ^{13}C NMR, IR spectroscopy and HRMS or MALDI-TOF-MS (see the ESI†).

Photophysical properties

The UV-vis absorption spectra of the dyes measured in dichloromethane and on TiO_2 films are shown in Fig. 2. The detailed parameters are summarized in Table 1. All the dyes showed two major absorption bands. The absorption band at 300–400 nm is attributed to the π–π* transition of the conjugated system and the absorption band at 400–670 nm is ascribed to the intramolecular charge transfer (ICT) from the functionalized triphenylamine donor to the cyanoacetic acid acceptor. Compared with the single D–π–A dye **AZ6**, the double D–π–A dye **A6** exhibited broader absorption characteristics with a higher molar extinction coefficient (ε) in the whole absorption region due to conjugation extension. It is worth noting that the π–π* electron transition band of the three D–π–A dyes showed a higher ε than their ICT bands, which indicated that a stronger π–π* interaction occurred in the dyes due to the bulky donor configuration. This phenomenon can also be found in other reported dyes.[34,43,44] Dye **A8** showed a narrower and less intense ICT band than **A9**, which was caused by the poor coplanarity of the π-spacer and the *meta*-position acceptor molecular configuration may weaken the charge transfer. When the phenyl ring was replaced with a thiophene group, the absorption properties of sensitizer **A6** were further enhanced. The ε values at λ_{max} of the absorption spectra for **A6**, **A8**, and **A9** were 56 210 M^{-1} cm^{-1}, 34 556 M^{-1} cm^{-1}, and 41 648 M^{-1} cm^{-1}, respectively, suggesting that the absorption characteristics can be effectively fine-tuned by adjustment of the π-spacer segments and the acceptor position.

In the case of the dyes absorbed on the TiO_2 surface, the absorption bands were broader and red-shifted (*ca.* 50 nm) than those in solution, which is favorable to improving the light-harvesting ability. In order to further verify the binding mode of the sensitizers on the TiO_2 film, the FT-IR analysis of the dyes anchored on the TiO_2 film was carried out.[45] As shown in Fig. S2 (ESI†), asymmetric stretching (υ_{as}, around 1598 cm^{-1}) and symmetric stretching (υ_s, around 1408 cm^{-1}) bands appeared, whereas the –COOH peak (around 1724 cm^{-1}) of the pure dyes disappeared. This result indicates that all three double D–π–A dyes adsorbed on the TiO_2 film in the bidentate adsorption mode, which may improve the affinity of the dye to

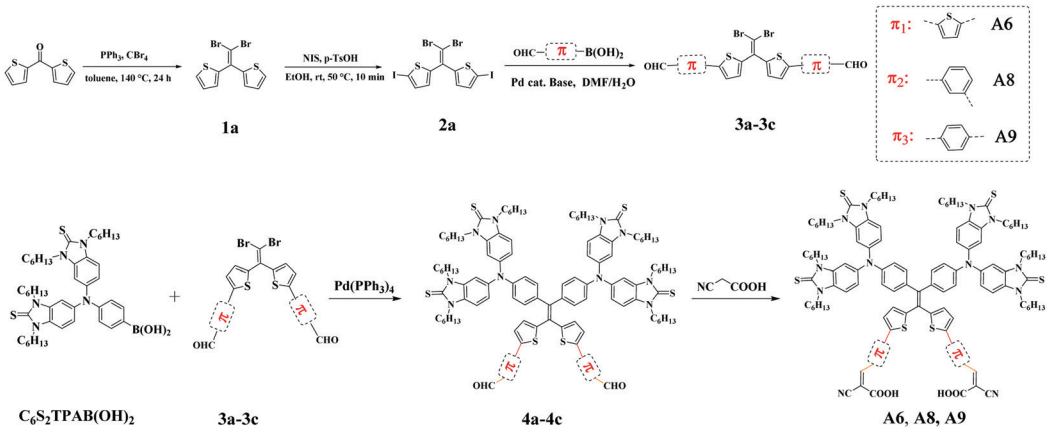

Scheme 1 Synthetic routes of dyes **A6**, **A8**, and **A9**.

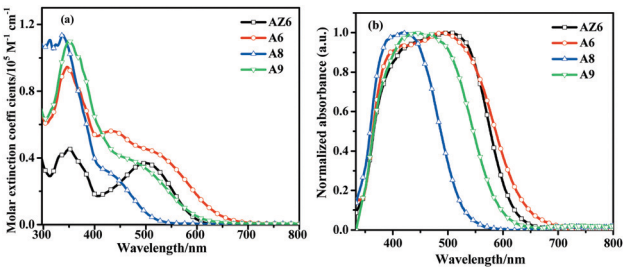

Fig. 2 UV-vis absorption spectra of the dyes (a) in CH_2Cl_2 solution and (b) on the TiO_2 film.

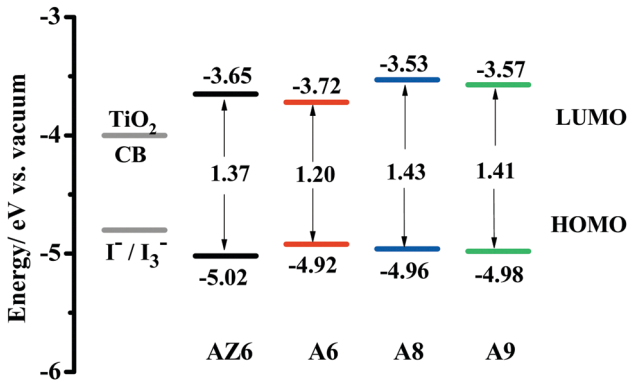

Fig. 3 CV-derived HOMO and LUMO energy levels of the dyes.

Table 1 Photophysical and electrochemical properties of the dyes

Dye	λ_{max}[a] (nm)	ε[a] (M^{-1} cm^{-1})	E_{ox}[b] (eV)	E_{red}[b] (eV)	E_{HOMO}[b] (eV)	E_{LUMO}[b] (eV)	E_g[b] (eV)
A6	432	56 210	0.21	−0.99	−4.92	−3.72	1.20
	484	47 420					
A8	413	34 556	0.25	−1.18	−4.96	−3.53	1.43
A9	447	41 648	0.27	−1.14	−4.98	−3.57	1.41
AZ6	501	36 939	0.31	−1.06	−5.02	−3.65	1.37

[a] Absorption spectra of sensitizers in CH_2Cl_2 (10^{-5} M). [b] $E_{HOMO} = -e(E_{ox} + 4.71)$ (eV) and $E_{LUMO} = -e(E_{red} + 4.71)$ (eV); $E_g = e(E_{ox} - E_{red})$ (eV).

the TiO_2 film. The desorption experiment[25] of the dyes in an alkaline solution (Fig. S3, ESI†) showed that the di-anchoring dyes were more difficult to extract than the mono-anchoring dyes. The result is consistent with its binding mode.

Electrochemical properties

Cyclic voltammetry (CV) was performed to evaluate the feasibility of the electron injection and dye regeneration processes.[46] As shown in Fig. 3, all dyes had sufficiently high LUMO levels, which indicates that electrons can be effectively injected from the excited dyes into the conduction band of TiO_2 (−4.0 eV *vs.* vacuum). Meanwhile, the HOMO levels of the dyes were more negative than the redox potential of the iodide/triiodide electrolyte (−4.80 eV *vs.* vacuum), ensuring that these oxidized dyes could be easily regenerated. For **A8** and **A9**, similar energy levels demonstrate that the acceptor position has a slight influence on the energy levels. Replacing the phenyl with a thiophene ring, the LUMO level of dye **A6** significantly shifted down, thus leading to a narrow energy gap, which may be favorable for generating a higher photocurrent. The HOMO–LUMO energy gap values decreased in the order: **A8** (1.43 eV) > **A9** (1.41 eV) > **AZ6** (1.37 eV) > **A6** (1.20 eV), which is consistent with the absorption characteristics.

DFT calculations

The molecular geometry conformations and electronic properties of dyes **A6–A9** were simulated by density functional theory (DFT) and time-dependent density functional theory (TD-DFT). The frontier molecular orbitals of the dyes are shown in Fig. 4 and the corresponding energy levels are listed in Table S2 (ESI†). Compared with **A9**, **A8** presents a more twisted molecular configuration and a shorter distance between the two acceptors (13.9 Å for **A8** and 20.0 Å for **A9**), which has an advantage in inhibiting charge recombination. In contrast, **A6** shows better coplanarity from the bithiophene to the acceptor, which is favorable for its effective intramolecular charge transfer process. The HOMO levels of the three dyes are mainly

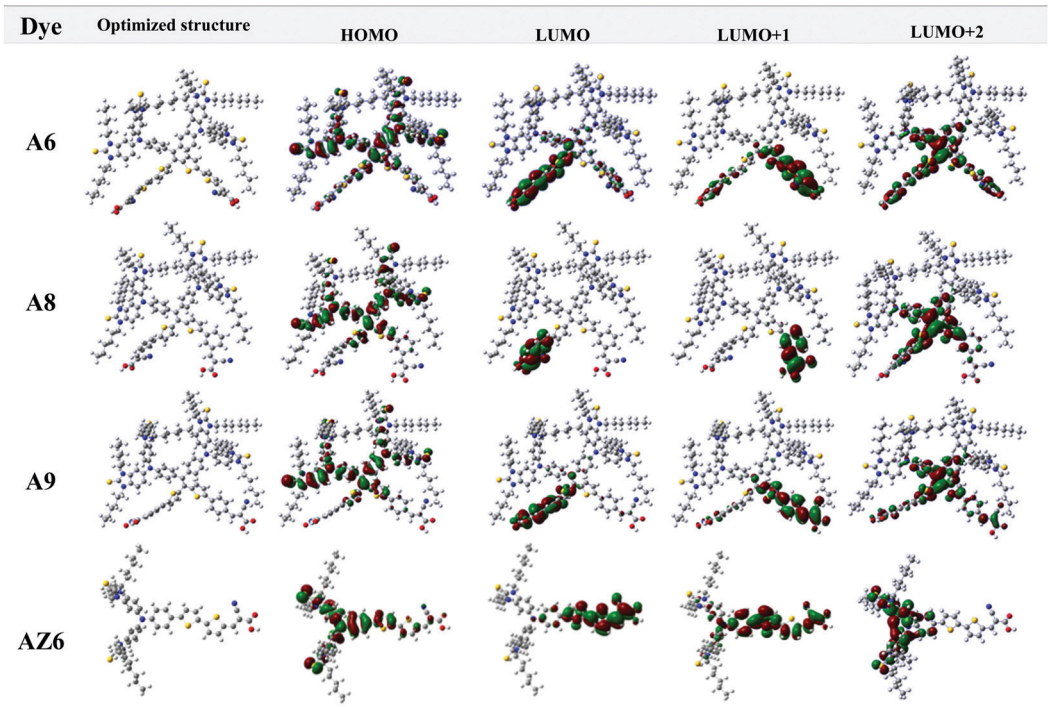

Fig. 4 Frontier molecular orbitals of dyes **A6**, **A8**, **A9**, and **AZ6**.

concentrated on the donor moieties. For di-anchoring dyes, the charges are mainly located on both sides of their two branches, implying double electron injection channels. According to TD-DFT theoretical calculations, the ICT in **A8** and **A9** is largely from the HOMO to LUMO+2 (Table S3, ESI†), while for **A6** is largely from the HOMO to the LUMO.

Photovoltaic performance of DSSCs

The DSSC performances of the dyes were evaluated under simulated AM 1.5G solar light (100 mW cm^{-2}) and the relevant parameters are tabulated in Table 2. The photocurrent density–voltage (*J–V*) curves and incident photon to current conversion efficiency (IPCE) spectra are plotted in Fig. 5. The J_{SC} values increased in the sequence: **A8** (10.26 mA cm^{-2}) < **A9** (16.60 mA cm^{-2}) < **AZ6** (16.84 mA cm^{-2}) < **A6** (18.63 mA cm^{-2}). Obviously, the **A8**-based DSSC displayed an inferior photocurrent, although **A8** has a higher loading amount (0.74×10^{-7} mol cm^{-2}) than **A6**. This result indicates that the loading amount has a small influence on its photocurrent as observed in other reported dyes.[47,48] The narrow UV-vis absorption band of **A8** in solution and on the TiO_2 film is consistent with the integration and intensity of the IPCE spectrum. All the factors contribute to a low J_{SC} value of **A8**. It is worth noting that the V_{OC} values showed an opposite tendency: **A8** (731.8 mV) > **A9** (717 mV) > **AZ6** (683.7 mV) > **A6** (647.0 mV). Also compared with the mono-anchoring dye **AZ6**, the **A6**-based DSSC showed a lower V_{OC}, which may be caused by the following two aspects. Firstly, compared with the mono-anchoring dye **AZ6** (0.84×10^{-7} mol cm^{-2}), the di-anchoring dye **A6** released more protons ($2 \times 0.51 \times 10^{-7}$ mol cm^{-2}) to the TiO_2 surface and thus decreased the E_{CB} of the TiO_2. Furthermore, the dye **A6** with more active sulfur sites is easier to form dye–iodine complexes,[49,50] causing serious charge recombination. However, replacing the thiophene with a phenyl ring in the π-spacer, higher V_{OC} values were observed in both **A8**- and **A9**-based DSSCs. Compared with dyes **AZ6** and **A6**, dyes **A8** and **A9** have a better loading capacity, indicating that more protons were released and then the V_{OC} was decreased. The higher V_{OC} values indicate that the benzene ring in the π-spacer effectively inhibits charge recombination and then reduces dark current. The DSSC based on **A8** showed a slightly higher V_{OC} value than that based on **A9**, which may be due to the larger steric hindrance. This reasonable speculation is also supported by the dark current test results (Fig. 5). Overall, the DSSC based on **A6** obtained a power conversion

Table 2 Photovoltaic parameters of the DSSCs based on **A6**, **A8**, **A9** and **AZ6**[a]

Dye	J_{SC} (mA cm^{-2})	V_{OC} (mV)	FF	PCE (%)	Dye loading (10^{-7} mol cm^{-2})
A6	18.63 (18.11 ± 0.96)	647.0 (648.2 ± 7.5)	0.68 (0.69 ± 0.01)	8.21 (8.08 ± 0.32)	0.51
A8	10.26 (10.01 ± 0.26)	731.8 (733.0 ± 6.7)	0.71 (0.71 ± 0.01)	5.36 (5.23 ± 0.15)	0.74
A9	16.60 (16.36 ± 0.47)	717.0 (712.0 ± 9.4)	0.68 (0.69 ± 0.01)	8.14 (8.05 ± 0.11)	0.91
AZ6	16.84 (16.84 ± 0.50)	683.7 (689.0 ± 20.2)	0.72 (0.71 ± 0.02)	8.31 (8.24 ± 0.27)	0.84

[a] Performances of DSSCs were measured with a 0.25 cm^2 working area under AM 1.5G solar light irradiation (100 mW cm^{-2}), the TiO_2 layer thickness is 13 μm and the photovoltaic data are the averaged values of six parallel cells.

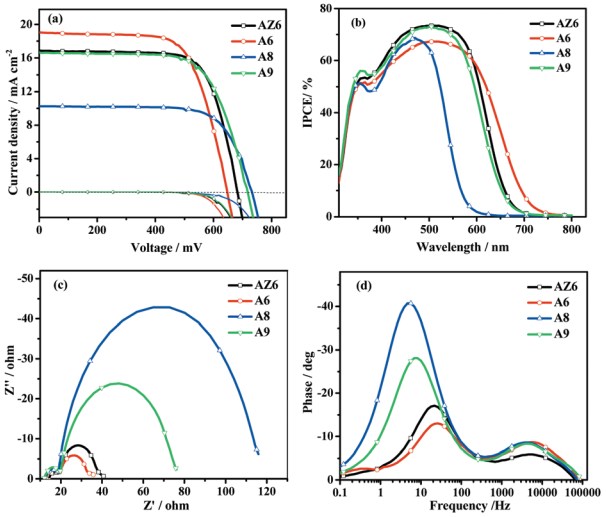

Fig. 5 Device characterization of DSSCs based on organic dyes **AZ6**, **A6**, **A8** and **A9** with the iodide liquid electrolyte: (a) *J*–*V* plots (measured under one sun or dark conditions); (b) IPCE spectra; and (c) Nyquist and (d) Bode plots (measured in the dark).

efficiency (PCE = 8.21%) with the highest photocurrent. When the acceptor position was altered from the *meta*- to the *para*-position, the efficiency increased by 52% from **A8** (PCE = 5.36%) to **A9** (PCE = 8.14%), which confirmed that the suitable acceptor position is crucial for the device performance. The **A6**-based DSSC presented a broad spectral response and extended the spectral region to 750 nm. The integration area of the IPCE spectra of the three dyes is in good accordance with the light-harvesting characteristics and J_{SC} values.

In addition to the PCE of the DSSCs, the stability of the dye-based DSSCs was also evaluated to further reveal the differences between mono-anchoring dyes and di-anchoring dyes. The cells were stored at room temperature and approximately 25% relative humidity. Fig. S6 (ESI†) shows the variation of the photovoltaic parameters of DSSCs recorded under continuous light irradiation (AM 1.5G, 100 mW cm^{-2}) over a period of 3000 h. The **A6**-based solar cell showed the best long-term stability, which can still retain 98% of the initial value after 3000 h. After 3000 hours of aging, the **A8**-based solar cell and **A9**-based solar cell retained 90% and 82% of the initial efficiencies, respectively. As a comparison, the **AZ6**-based solar cell could retain 78% of its initial value after 3000 h of one sun soaking. This result confirms that the bidentate binding mode of di-anchoring dyes is beneficial for enhancing the stability of DSSCs.

Electrochemical impedance spectroscopy

Electrochemical impedance spectroscopy (EIS) analysis was performed to investigate the photovoltaic properties and charge transfer processes at the electrode/electrolyte interface of DSSCs under dark conditions. As shown in Fig. 5, the charge-transfer resistance at the dye-adsorbed TiO_2/electrolyte interface was assessed through the diameter of the semicircle. The diameter of the semicircle increased in the order: **A6** < **AZ6** < **A9** < **A8**. The electron recombination lifetime (τ_e) was obtained from the Bode phase plot (Fig. 5d) using the equation $\tau_e = 1/2\pi f_{max}$, which increased in the order: **A6** (6.5 ms) < **AZ6** (8.0 ms) < **A9** (21.3 ms) < **A8** (29.9 ms). The larger semicircle and longer lifetime imply less interfacial charge recombination. The results coincided well with the V_{OC} values and dark current test results, which further confirmed that the phenyl ring effectively retarded the charge recombination process.

Conclusions

We synthesized three **DPDT**-based double D–π–A organic sensitizers by altering the terminal fragment. The di-anchoring sensitizers showed robust affinity to the TiO_2 surface and better long-term stability than the corresponding mono-anchoring dye **AZ6**. Owing to the extension of conjugation, the **A6**-based DSSC achieved a high photocurrent. By altering the terminal fragment of the dyes, the photocurrent and voltage can be improved. As a result, the **A6**-based DSSC achieved an efficiency of 8.21% with a superior J_{SC} of 18.63 mA cm^{-2}. When replacing the terminal thiophene with a phenyl ring, the **A9**-based DSSC yielded a comparable efficiency of 8.14% with a higher V_{OC} value of 717 mV. Further study on new double D–π–A sensitizers through a molecular engineering strategy is in progress.

Conflicts of interest

There are no conflicts to declare.

Acknowledgements

We acknowledge the financial support from the National Science Foundation Committee of China (21673134 and 21543012), Program for Science & Technology Innovation Team of Shaanxi Province (2018TD-030), the International Science and Technology Cooperation Project of Shaanxi Province (2021KW-20) and the Fundamental Research Funds for the Central Universities (GK202101005).

References

1 S. Zhang, X. Yang, Y. Numata and L. Han, *Energy Environ. Sci.*, 2013, **6**, 1443–1464.
2 K. Zeng, Z. Tong, L. Ma, W.-H. Zhu, W. Wu and Y. Xie, *Energy Environ. Sci.*, 2020, **13**, 1617–1657.
3 N. Zhou, K. Prabakaran, B. Lee, S. H. Chang, B. Harutyunyan, P. Guo, M. R. Butler, A. Timalsina, M. J. Bedzyk, M. A. Ratner, S. Vegiraju, S. Yau, C.-G. Wu, R. P. H. Chang, A. Facchetti, M.-C. Chen and T. J. Marks, *J. Am. Chem. Soc.*, 2015, **137**, 4414–4423.
4 L. Zhang, X. Yang, W. Wang, G. G. Gurzadyan, J. Li, X. Li, J. An, Z. Yu, H. Wang, B. Cai, A. Hagfeldt and L. Sun, *ACS Energy Lett.*, 2019, **4**, 943–951.

5 J. An, X. Yang, B. Cai, L. Zhang, K. Yang, Z. Yu, X. Wang, A. Hagfeldt and L. Sun, *ACS Appl. Mater. Interfaces*, 2020, **12**, 46397–46405.
6 H. Song, Q. Liu and Y. Xie, *Chem. Commun.*, 2018, **54**, 1811–1824.
7 Y. Kurumisawa, T. Higashino, S. Nimura, Y. Tsuji, H. Iiyama and H. Imahori, *J. Am. Chem. Soc.*, 2019, **141**, 9910–9919.
8 J. Zou, Q. Yan, C. Li, Y. Lu, Z. Tong and Y. Xie, *ACS Appl. Mater. Interfaces*, 2020, **12**, 57017–57024.
9 C.-Y. Chen, M. Wang, J.-Y. Li, N. Pootrakulchote, L. Alibabaei, C.-H. Ngoc-le, J.-D. Decoppet, J.-H. Tsai, C. Grätzel, C.-G. Wu, S. M. Zakeeruddin and M. Grätzel, *ACS Nano*, 2009, **3**, 3103–3109.
10 S. Mathew, A. Yella, P. Gao, R. Humphry-Baker, B. F. E. Curchod, N. Ashari-Astani, I. Tavernelli, U. Rothlisberger, M. K. Nazeeruddin and M. Grätzel, *Nat. Chem.*, 2014, **6**, 242–247.
11 K. Zeng, W. Tang, C. Li, Y. Chen, S. Zhao, Q. Liu and Y. Xie, *J. Mater. Chem. A*, 2019, **7**, 20854–20860.
12 K. Zeng, Y. Chen, W.-H. Zhu, H. Tian and Y. Xie, *J. Am. Chem. Soc.*, 2020, **142**, 5154–5161.
13 H. Meier, Z.-S. Huang and D. Cao, *J. Mater. Chem. C*, 2017, **5**, 9828–9837.
14 Z. Wang, L. Miu, H. Yao, M. Liang, S. Yan, J. Wang, T. Guo, L. Zhang, J. Chen and S. Xue, *Dyes Pigm.*, 2019, **162**, 126–135.
15 Y.-F. Chen, J.-M. Liu, J.-F. Huang, L.-L. Tan, Y. Shen, L.-M. Xiao, D.-B. Kuang and C.-Y. Su, *J. Mater. Chem. A*, 2015, **3**, 8083–8090.
16 A. Abbotto, N. Manfredi, C. Marinzi, F. De Angelis, E. Mosconi, J.-H. Yum, Z. Xianxi, M. K. Nazeeruddin and M. Grätzel, *Energy Environ. Sci.*, 2009, **2**, 1094–1101.
17 Z.-S. Huang, C. Cai, X.-F. Zang, Z. Iqbal, H. Zeng, D.-B. Kuang, L. Wang, H. Meier and D. Cao, *J. Mater. Chem. A*, 2015, **3**, 1333–1344.
18 X. Jiang, K. M. Karlsson, E. Gabrielsson, E. M. J. Johansson, M. Quintana, M. Karlsson, L. Sun, G. Boschloo and A. Hagfeldt, *Adv. Funct. Mater.*, 2011, **21**, 2944–2952.
19 W. Lee, S. B. Yuk, J. Choi, H. J. Kim, H. W. Kim, S. H. Kim, B. Kim, M. J. Ko and J. P. Kim, *Dyes Pigm.*, 2014, **102**, 13–21.
20 C.-Y. Lo, D. Kumar, S.-H. Chou, C.-H. Chen, C.-H. Tsai, S.-H. Liu, P.-T. Chou and K.-T. Wong, *ACS Appl. Mater. Interfaces*, 2016, **8**, 27832–27842.
21 X. Ren, S. Jiang, M. Cha, G. Zhou and Z.-S. Wang, *Chem. Mater.*, 2012, **24**, 3493–3499.
22 Y. Hong, J.-Y. Liao, D. Cao, X. Zang, D.-B. Kuang, L. Wang, H. Meier and C.-Y. Su, *J. Org. Chem.*, 2011, **76**, 8015–8021.
23 H.-T. Feng, Y.-X. Yuan, J.-B. Xiong, Y.-S. Zheng and B. Z. Tang, *Chem. Soc. Rev.*, 2018, **47**, 7452–7476.
24 F. Zhang, J. Fan, H. Yu, Z. Ke, C. Nie, D. Kuang, G. Shao and C. Su, *J. Org. Chem.*, 2015, **80**, 9034–9040.
25 C.-T. Li, Y.-L. Kuo, C. H. P. Kumar, P.-T. Huang and J. T. Lin, *J. Mater. Chem. A*, 2019, **7**, 23225–23233.
26 Y.-Q. Yan, Y.-Z. Zhu, J. Han, P.-P. Dai, M. Yan and J.-Y. Zheng, *Dyes Pigm.*, 2020, **183**, 108630.
27 C.-T. Li, F.-L. Wu, C.-J. Liang, K.-C. Ho and J. T. Lin, *J. Mater. Chem. A*, 2017, **5**, 7586–7594.
28 D. Heredia, J. Natera, M. Gervaldo, L. Otero, F. Fungo, C.-Y. Lin and K.-T. Wong, *Org. Lett.*, 2010, **12**, 12–15.
29 G. Pozzi, S. Orlandi, M. Cavazzini, D. Minudri, L. Macor, L. Otero and F. Fungo, *Org. Lett.*, 2013, **15**, 4642–4645.
30 X. Qian, H.-H. Gao, Y.-Z. Zhu, L. Lu and J.-Y. Zheng, *RSC Adv.*, 2015, **5**, 4368–4375.
31 G. Tian, S. Cai, X. Li, H. Ågren, Q. Wang, J. Huang and J. Su, *J. Mater. Chem. A*, 2015, **3**, 3777–3784.
32 J. He, F. Guo, X. Li, W. Wu, J. Yang and J. Hua, *Chem. – Eur. J.*, 2012, **18**, 7903–7915.
33 W. Ying, J. Yang, M. Wielopolski, T. Moehl, J.-E. Moser, P. Comte, J. Hua, S. M. Zakeeruddin, H. Tian and M. Grätzel, *Chem. Sci.*, 2014, **5**, 206–214.
34 R. Yeh-Yung Lin, F.-L. Wu, C.-H. Chang, H.-H. Chou, T.-M. Chuang, T.-C. Chu, C.-Y. Hsu, P.-W. Chen, K.-C. Ho, Y.-H. Lo and J. T. Lin, *J. Mater. Chem. A*, 2014, **2**, 3092–3101.
35 S. Qu, W. Wu, J. Hua, C. Kong, Y. Long and H. Tian, *J. Phys. Chem. C*, 2010, **114**, 1343–1349.
36 A. Yella, C.-L. Mai, S. M. Zakeeruddin, S.-N. Chang, C.-H. Hsieh, C.-Y. Yeh and M. Grätzel, *Angew. Chem., Int. Ed.*, 2014, **53**, 2973–2977.
37 S. Haid, M. Marszalek, A. Mishra, M. Wielopolski, J. Teuscher, J.-E. Moser, R. Humphry-Baker, S. M. Zakeeruddin, M. Grätzel and P. Bäuerle, *Adv. Funct. Mater.*, 2012, **22**, 1291–1302.
38 R. B. Ambre, S. B. Mane, G.-F. Chang and C.-H. Hung, *ACS Appl. Mater. Interfaces*, 2015, **7**, 1879–1891.
39 J. Rochford, D. Chu, A. Hagfeldt and E. Galoppini, *J. Am. Chem. Soc.*, 2007, **129**, 4655–4665.
40 A. S. Hart, C. B. Kc, H. B. Gobeze, L. R. Sequeira and F. D'Souza, *ACS Appl. Mater. Interfaces*, 2013, **5**, 5314–5323.
41 S. Liu, Y. Jiao, Y. Ding, X. Fan, J. Song, B. Mi and Z. Gao, *Dyes Pigm.*, 2020, **180**, 108470.
42 Z. Wu, Z. An, X. Chen and P. Chen, *Org. Lett.*, 2013, **15**, 1456–1459.
43 X. Lu, X. Jia, Z.-S. Wang and G. Zhou, *J. Mater. Chem. A*, 2013, **1**, 9697–9706.
44 X.-X. Dai, H.-L. Feng, Z.-S. Huang, M.-J. Wang, L. Wang, D.-B. Kuang, H. Meier and D. Cao, *Dyes Pigm.*, 2015, **114**, 47–54.
45 M. C. Sil, V. Sudhakar, M. F. Mele Kavungathodi, V. Punitharasu and J. Nithyanandhan, *ACS Appl. Mater. Interfaces*, 2017, **9**, 34875–34890.
46 J. Hou, Z. a. Tan, Y. Yan, Y. He, C. Yang and Y. Li, *J. Am. Chem. Soc.*, 2006, **128**, 4911–4916.
47 H. Li, Y. Hou, Y. Yang, R. Tang, J. Chen, H. Wang, H. Han, T. Peng, Q. Li and Z. Li, *ACS Appl. Mater. Interfaces*, 2013, **5**, 12469–12477.
48 X.-F. Zang, T.-L. Zhang, Z.-S. Huang, Z. Iqbal, D.-B. Kuang, L. Wang, H. Meier and D. Cao, *Dyes Pigm.*, 2014, **104**, 89–96.
49 Y. Cui, Y. Wu, X. Lu, X. Zhang, G. Zhou, F. B. Miapeh, W. Zhu and Z.-S. Wang, *Chem. Mater.*, 2011, **23**, 4394–4401.
50 M. Zhang, J. Liu, Y. Wang, D. Zhou and P. Wang, *Chem. Sci.*, 2011, **2**, 1401–1406.